Annals of Biomedical Engineering, Vol. 44, No. 11, November 2016 (© 2016) pp. 3335–3345
DOI: 10.1007/s10439-016-1659-6

Near Infrared Spectroscopic Mapping of Functional Properties of Equine Articular Cartilage

JAAKKO K. SARIN,[1,2] MICHAEL AMISSAH,[3] HAROLD BROMMER,[4] DAVID ARGÜELLES,[5] JUHA TÖYRÄS,[1,2] and ISAAC O. AFARA[1,2,6]

[1]Department of Applied Physics, University of Eastern Finland, Kuopio, Finland; [2]Diagnostic Imaging Center, Kuopio University Hospital, Kuopio, Finland; [3]Department of Physics and Mathematics, University of Eastern Finland, Joensuu, Finland; [4]Department of Equine Sciences, Utrecht University, Utrecht, Netherlands; [5]School of Veterinary Medicine, Veterinary Teaching Hospital, University of Helsinki, Helsinki, Finland; and [6]Department of Electrical and Computer Engineering, Elizade University, Ondo, Nigeria

(*Received 14 January 2016; accepted 20 May 2016; published online 27 May 2016*)

Associate Editor Kent Leach oversaw the review of this article.

Abstract—Mechanical properties of articular cartilage are vital for normal joint function, which can be severely compromised by injuries. Quantitative characterization of cartilage injuries, and evaluation of cartilage stiffness and thickness by means of conventional arthroscopy is poorly reproducible or impossible. In this study, we demonstrate the potential of near infrared (NIR) spectroscopy for predicting and mapping the functional properties of equine articular cartilage at and around lesion sites. Lesion and non-lesion areas of interests (AI, $N = 44$) of equine joints ($N = 5$) were divided into grids and NIR spectra were acquired from all grid points ($N = 869$). Partial least squares (PLS) regression was used to investigate the correlation between the absorbance spectra and thickness, equilibrium modulus, dynamic modulus, and instantaneous modulus at the grid points of 41 AIs. Subsequently, the developed PLS models were validated with spectral data from the grid points of 3 independent AIs. Significant correlations were obtained between spectral data and cartilage thickness ($R^2 = 70.3\%$, $p < 0.0001$), equilibrium modulus ($R^2 = 67.8\%$, $p < 0.0001$), dynamic modulus ($R^2 = 68.9\%$, $p < 0.0001$) and instantaneous modulus ($R^2 = 41.8\%$, $p < 0.0001$). Relatively low errors were observed in the predicted thickness (5.9%) and instantaneous modulus (9.0%) maps. Thus, if well implemented, NIR spectroscopy could enable arthroscopic evaluation and mapping of cartilage functional properties at and around lesion sites.

Keywords—Spectroscopy, Biomechanical, Indentation, Partial least squares (PLS) regression.

Address correspondence to Jaakko K. Sarin, Department of Applied Physics, University of Eastern Finland, Kuopio, Finland. Electronic mail: jaakko.sarin@uef.fi

INTRODUCTION

Articular cartilage is a protective, avascular, and aneural tissue allowing near frictionless motion in diarthrodial joints.[34] The main components of articular cartilage include water (65–80%) and a solid macromolecular framework of collagen fibers (10–30%) and proteoglycans (PG, 3–10%).[12,28,34] Localized injuries of articular cartilage may cause increased loading of areas around the injury, making the surrounding cartilage more vulnerable to further damage.[12,13,34] This increased loading often leads to progressive structural and compositional deterioration, thus resulting in the development of post-traumatic osteoarthritis (OA),[12,34] which is characterized by loss of cartilage, pain, and restriction in joint movement.[21] Changes in cartilage structure, during progression of OA, results in alteration of the tissue's ability to withstand physiological loads which often leads to further damage if not treated.[12,13,34]

Arthroscopic surgery is usually used to confirm and repair joint injuries, which are pre-diagnosed with computed tomography or magnetic resonance imaging.[8,48] However, arthroscopic evaluation of cartilage injuries is subjective and has poor intra- and inter-observer reliability.[42,43] Furthermore, sub-surface lesions and cracks may be unnoticed by the surgeon. During surgery, the biomechanical response of cartilage is evaluated by probing the tissue surface with an arthroscopic hook, which enables detection of chondral softening around local cartilage defects. This is a subjective technique and may not give the true representation of the tissue health. In laboratory environ-

ment, indentation test is considered the gold standard for determining the biomechanical properties of cartilage.[25,26] A number of hand-held arthroscopic indentation devices have been developed for evaluation of cartilage properties *in vivo*. Unfortunately, these devices are limited by poor reproducibility.[11,30] Thus, a more objective method, such as NIR, for evaluating cartilage health during surgery is required.

Several rapid non-destructive techniques are currently being researched for evaluation of cartilage integrity in real-time, such as ultrasound imaging,[22,40] optical coherence tomography (OCT),[15,46] near infrared (NIR) spectroscopy,[4,41,44] mid infrared (MIR) spectroscopy,[20,50] and Raman spectroscopy.[17,45] In this study, we adopt NIR spectroscopy to evaluate articular cartilage health. NIR light penetrates deep into the cartilage matrix and the diffusely reflected light is measured and analyzed relative to transmitted light.[41] Recent studies have shown that the integrity of cartilage matrix affects its optical response, which is mainly characterized by the chemical bonds CH, NH, OH and SH [2,4,35,41]—the predominant bond types in biological tissues. In previous studies, the NIR spectrum of cartilage has been shown to correlate with its thickness,[3,33,35] composition,[2,6,9,33,36] biomechanical properties[5] and histological grading,[1,4,5,33,41] thus demonstrating the potential of NIR spectroscopy to detect changes associated with early stage cartilage degeneration, including superficial PG loss and collagen disruption.[6] Application of NIR for spatial mapping of cartilage PG content has also been attempted.[6] However, no study has investigated the capacity of NIR to map cartilage functional properties at and around lesions, therefore enabling the assessment of the extent of damaged cartilage to be repaired during arthroscopic surgery.[24]

In the current study, we hypothesized that NIR spectroscopic mapping of cartilage functional properties would be indicative of cartilage lesions and chondral softening. To test this hypothesis, multivariate statistical technique of PLS regression was used to develop calibration models between articular cartilage spectral data and the reference data: cartilage thickness and biomechanical properties. The models were then used to predict the properties of an independent group of AIs and compared with the measured reference values. Finally, an independent AI was mapped using the measured and predicted values.

MATERIALS AND METHODS

Sample Preparation

Metacarpophalangeal joints extracted from mature horses ($N = 5$) were obtained from a slaughterhouse (Equine Slaughter House Van de Veen, Nijkerk, Netherlands) and used in this study, for this reason no ethical permission was needed. The intact and damaged areas of interests (AI, $N = 44$) were selected by two board certified qualified equine surgeons (Diplomate European College of Veterinary Surgeons, Brommer H. & Argüelles D.). The blind coded AIs were scored twice arthroscopically and independently by both surgeons according to the international cartilage repair society (ICRS) scoring system[10] to differentiate healthy ($N = 19$) and damaged ($N = 25$) AIs.

The anatomical locations were enclosed with a marker (15 × 15 mm blocks) on the surface of articular cartilage and divided uniformly into grids of 25 points (Fig. 1a). Sample geometry and locations of AIs limited the number of measurement locations. Additionally, several points ($N = 15$) with fully eroded cartilage and exposed subchondral bone were excluded due to the inability to obtain biomechanical measurements of cartilage. A total of 869 points were measured with NIR spectroscopy and reference methods.

NIR Spectroscopy

NIR diffuse reflectance spectroscopy was utilized to optically probe the AIs. The NIR instrumentation consists of a halogen light source (wavelength 360–2500 nm, power 5 W, optical power 239 μW in a 600 μm fiber, Avantes BW, Apeldoorn, Netherlands), a spectrometer (wavelength 200–1160 nm, AvaSpec-ULS2048XL, Avantes BW, Apeldoorn, Netherlands), and a diffuse reflectance fiber optic probe. The probe ($d = 5$ mm) consists of seven fibers ($d_{\text{fiber}} = 600$ μm) within the central window ($d = 2$ mm). Six of the fibers were used for transmitting the NIR light, and the central fiber was used for collecting the reflected light from the sample. Data storage and online monitoring were managed with a personal computer running Avasoft 8.0 software (Avantes BW, Apeldoorn, Netherlands). The integration time ($t = 90$ ms) was optimized for the hardware to maximize the signal-to-noise ratio without saturation. Dark spectra was collected with the light source off to eliminate environmental factors such as stray light, and reference spectra was acquired prior to measurements from a reflectance standard (Spectralon, SRS-99, Labsphere Inc., North Sutton, USA) with the fiber optic probe perpendicular and in contact with the reflectance standard. The absorbance spectrum (A_λ) was calculated using the Beer-Lambert's law[14] and taking into account the environmental factors.

$$A_\lambda = -\log_{10}((S_\lambda - D_\lambda)/(R_\lambda - D_\lambda)), \qquad (1)$$

where S_λ is the light reflected from the sample, D_λ the dark spectrum, and R_λ the reference spectrum.

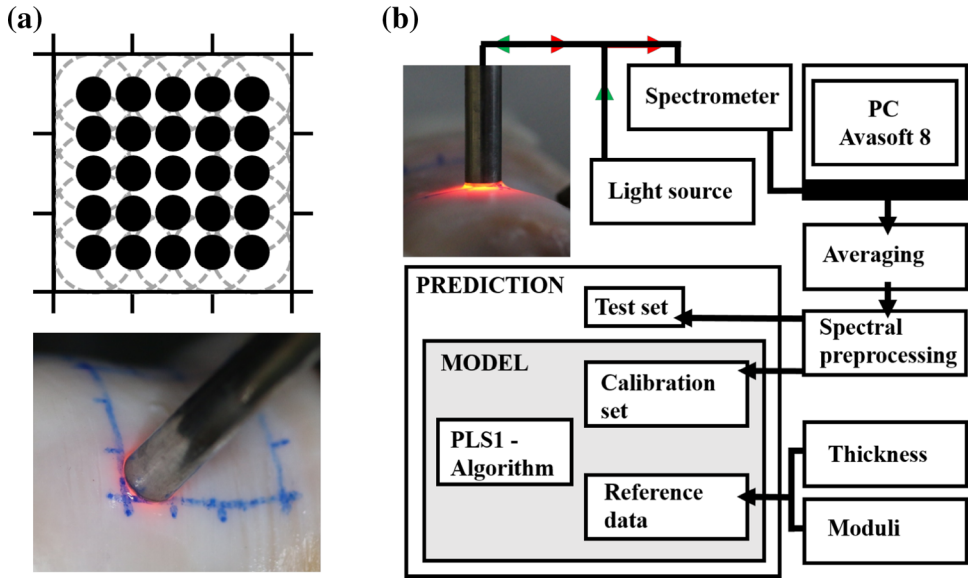

FIGURE 1. Mapping and alignment of the probe on cartilage surface (a) and the protocol for developing and validating PLS model between spectral data and reference measurements (b).

During measurement, the probe was oriented perpendicularly and kept in contact with the surface of the sample (Fig. 1a). Spectral measurement of each point was repeated three times by realigning the probe for each measurement. In each repetition, eight consecutive spectra were collected and averaged. The final spectrum was calculated as an average of the three repetitions. The coefficient of variation (CV) was calculated to determine the reproducibility of the spectral measurement. The CV[19] is defined as:

$$CV_\lambda = 100\% \times \sqrt{\sum_{j=1}^{N} CV_{\lambda,j}^2 / N} = 100\% \times \sqrt{\sum_{j=1}^{N} SD_{\lambda,j}^2 / (\bar{A}_{\lambda,j}^2 N)}, \quad (2)$$

where $SD_{\lambda,j}$ is the standard deviation of the three absorbance spectra and $\bar{A}_{\lambda,j}$ is the averaged absorbance spectrum. Spectral data in the wavelength region of 700–1150 nm was used for analyses (Fig. 1b). Physiological condition was preserved by constantly spraying the cartilage surface with phosphate-buffered saline (PBS) and placing PBS soaked cloths around the measurement points. After NIR spectroscopy, the samples were submerged in PBS and stored at −20 ºC until prepared for the reference analyses.

Measurement of Cartilage Thickness

Prior to reference measurements, the samples were thawed in room temperature PBS for one hour. The AIs were imaged using OCT[15,46] (wavelength 1305 ± 55 nm, axial resolution <20 μm, lateral resolution 25–60 μm; Ilumien PCI Optimization System, St. Jude Medical, St. Paul, MN, USA) to determine the thickness of non-calcified cartilage. The measurements were performed with the samples fully immersed in PBS. The field of view of OCT is approximately 4 mm deep and due to light attenuation cartilage can only be visualised up to a depth of approximately 2 mm using OCT. Equine cartilage thickness ranges between 0.5 and 2.5 mm[29]; in this study, cartilage thickness varied between 0.32 and 1.82 mm, with average of 0.89 mm. OCT was performed first because information on cartilage thickness was needed for biomechanical tests.

Biomechanical Testing

After OCT measurements, the biomechanical properties of the samples were determined with indentation testing.[27] Before testing the upper metacarpal and lower phalanx sections of the joints, the sections were cut in half along the ridge and the groove, respectively. The cut samples were glued on a custom-made holder from the bone end, and the sample holder was mounted on a goniometer (#55-841, Edmund Optics Inc., Barrington, NJ, USA). The sample was fully immersed in PBS supplemented with Antibiotic-Antimycotic solution (A5955, Sigma-Aldrich) during measurements. A load cell, with force resolution of 5 mN (Sensotec, Columbus, OH, USA), and an actuator, with displacement resolution of 0.1 μm (PM500-1 A, Newport, Irvine, CA, USA), were used in biomechanical testing.[47] The sample surface

was aligned perpendicular to a plane-ended cylindrical indenter ($d = 0.53$ mm) by adjusting the goniometer. The indenter was driven into contact with the surface of the sample with pre-stress of 12.5 kPa.[27] Contact was ensured by indenting the specimen 2% of its thickness five times. Two different protocols were used for testing the cartilage samples. In the 1st protocol, three consecutive 7.5% strain steps were performed with 10 min relaxation time in between the steps, followed by 4 cycles of dynamic sinusoidal loading ($f = 1.0$ Hz) with amplitude of 2% of the remaining cartilage thickness. In the 2nd protocol, a single 7.5% strain step was used. The strain rate for both protocols was 100%/s relative to the thickness of the cartilage. For each AI, five grid points were systematically selected at and around the lesion and measured using the 1st protocol; the remaining points were measured along the 2nd protocol. Two protocols were used for the testing as applying only the 1st protocol, which is more detailed, on all points would be too time consuming, thus exposing the samples to the risk of deterioration. To guarantee successful indentation into cartilage, a 7.5% strain step was chosen based on existing studies[26,31] which utilized several 5.0% strain steps. In addition, the same strain step and rate were used in both protocols to ensure the results are comparable.

Moduli were calculated with solution derived from Hayes *et al.*[23]:

$$E = E_{\mathrm{m}}(1 - \nu^2)\pi a/(2\kappa h), \tag{3}$$

where E_{m} is the measured modulus, ν the Poisson's ratio, a the indenter radius, κ the theoretical correction factor, and h the sample thickness. Equilibrium and dynamic moduli were determined from the 1st protocol. Equilibrium modulus (E_{eq}) was determined from the linear slope of the equilibrium stress–strain curve.[25,26] Dynamic modulus (E_{dyn}) was calculated from sinusoidal loading as the ratio of stress and strain amplitudes at 1.0 Hz.[5,26] Instantaneous modulus (E_{in}) was determined from the first step of the stress-relaxation curves of both protocols. The following Poisson's ratios were used: equilibrium modulus ($\nu = 0.1$), dynamic modulus ($\nu = 0.5$), and instantaneous modulus ($\nu = 0.5$).[23,25,31]

Histological Staining

The AIs were prepared for histological analysis in order to qualitatively compare cartilage functional properties with compositional and structural changes. The samples were fixed in formalin, decalcified in EDTA and embedded in paraffin blocks. Three 5 μm thick slices were cut 5 mm apart and stained with Safranin-O according to standard protocols.[7]

Near Infrared Spectral Analysis

A multivariate statistical technique based on PLS regression was used to relate the multivariate spectral data to corresponding reference data of the samples. PLS regression is a bilinear regression method that finds the fundamental relations between predictor and response variables. These relations are usually explained by a small number of regression factors, which can be then used to predict response variables of new samples.[38,49] This multivariate technique was chosen as it enables analysis of data with strongly collinear and numerous variables (spectral information) and can simultaneously model several response variables, such as tissue properties.[5,7,9,20]

Prior to multivariate analysis, preprocessing of spectral data is often required to eliminate as much noise as possible without degrading essential information. The NIR spectra were smoothed with a third degree Savitzky-Golay filter with a window of 25 nm (40 points) to eliminate any background noise. The second derivative of the smoothed spectra was then calculated to remove baseline offset and the dominant linear term from the spectral data. Furthermore, second derivative spectral preprocessing allows specific identification of small and subtle absorption peaks which are not easily resolved visually in the original spectrum.[39] This was followed by additional smoothing with a 10 point moving average filter. Identical preprocessing was used in all analyses. Normalization methods, such as multiplicative scatter correction (MSC) and standard normal variate (SNV), were also used for spectral preprocessing.

The AIs were divided into two groups according to ICRS scores: healthy (ICRS 0) and damaged (ICRS 1 or higher) cartilage. The categorization was based on the average arthroscopy score of the surgeons. One healthy and two damaged AIs were selected for test validation and the remaining 41 AIs were used to construct the calibration model relating cartilage spectral data to the reference parameters. For thickness and instantaneous modulus, the PLS models were built with 799 and tested with 70 grid points, and for equilibrium and dynamic modulus with 202 and 15 grid points, respectively.

In the analysis, up to ten PLS components were tested. Cross-validation technique (k-fold, $k = 10$) was used in the development of the models. Since PLS1 algorithm is prone to under- and overfitting, this was avoided using test set validation by optimizing the number of components for the models with the minimum root mean square error of prediction (RMSEP) and the maximum R^2 of prediction of the test set. The optimal models were used to predict the properties of the test AIs from their preprocessed spectra and

compared to the measured values. Five to six PLS components were found to be optimal for the models. Outlier detection was performed by visual inspection of the spectral data, and inconsistent spectra ($N = 15$) were removed prior to reference analyses. These spectra correspond to locations with no cartilage layer. Additionally, existence of outlying spectra of each PLS model was investigated with the Hotelling's T^2 test, but no additional outliers were detected.

The measured and predicted thickness and instantaneous modulus values of single test AI with lesion was formatted as a matrix (5×5) to correspond with the grid points of the AI (Fig. 1a). Any negative predicted modulus value was replaced with the average of neighboring points. Cubic interpolation was used to increase the pixel density of the matrix up to 401×401 pixels prior to visualization. As a result of the time-consuming biomechanical protocol, the number of points for the equilibrium and dynamic moduli were limited; thus, these parameters were not mapped.

RESULTS

CV of spectral measurement in the optimal NIR region (700–1050 nm) was $0.82 \pm 0.32\%$. Variation between spectra of different measurements points was observed to be consistent with cartilage thickness (Fig. 2a). However, the difference with respect to thickness is not immediately apparent in the second derivative spectra (Fig. 2a: inset). On the other hand, differences in the second derivative data are consistent with variation in equilibrium modulus (Fig. 2b: inset). High correlations were observed between spectral data and cartilage reference data (thickness and biomechanical properties, Table 1, Figs. 3 and 4). Optimal correlation between spectral data and the reference biomechanical parameters was obtained with smoothing and second derivative transformation. No significant improvement in correlation was observed with MSC and SNV.

Mapping of the thickness and instantaneous modulus facilitated visualization of the distribution of these parameters (Fig. 5). In the test set, the average error between predicted and measured values for the thickness was 0.09 mm (5.9%), instantaneous modulus 1.89 MPa (9.0%), equilibrium modulus 0.80 MPa (14.9%), and dynamic modulus 3.30 MPa (14.3%) relative to the range of the reference variable. In the lesion AIs the variation of instantaneous modulus corresponds with the OCT and histological images.

DISCUSSION

In this study, for the first time, NIR spectroscopy was used to map the functional properties of cartilage around lesion sites. The combination of optical probing and the PLS1 algorithm allowed mapping of cartilage properties at and around the lesion sites, demonstrating its potential as a future arthroscopic method (Fig. 5). The developed PLS models predicted the non-calcified cartilage thickness and biomechanical properties of equine tissue with low errors (Figs. 3 and 4). The findings are consistent with previous studies where NIR was used to predict cartilage thickness[3,35] and biomechanical properties.[5,6] However, these studies have mainly focused on assessing cartilage properties at single locations e.g., lesion sites. To our knowledge, no studies mapping the biomechanical properties of articular cartilage around the lesion have been conducted. It is worth noting, that in earlier studies smaller sample size were used, restraining the analyses to the less accurate leave-one-out cross-validation technique. In this study, we have adopted the test set validation technique, which is more accurate in evaluating the performance of models.[1,20,37]

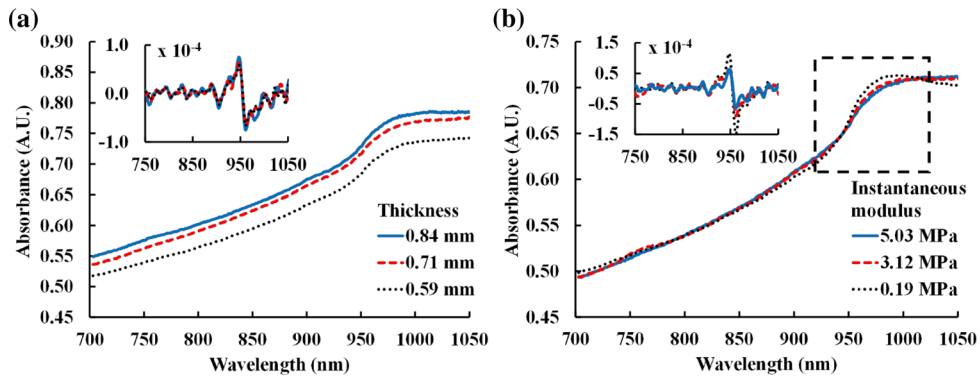

FIGURE 2. Representative raw absorbance and preprocessed (inset) absorbance spectra showing consistent variation with cartilage thickness (a) and instantaneous modulus (b). The spectra were chosen with identical modulus (a) or thickness (b) to clearly indicate differences. MSC was used to enhance the variation in spectra with changes in modulus, particularly between 925 and 1025 nm (b).

TABLE 1. The PLS regression statistics of NIR spectra and reference data.

				MODEL		TEST		
Response	Mean (CI)	Wavelength (nm)	C	R^2 (%)	RMSECV	R^2 (%)	RMSEP	Error (%)
Thickness (mm)	0.89 (0.87, 0.90)	700–1050	5	70.3	0.15	75.6	0.11	5.9
E_{in} (MPa)	4.76 (4.53, 4.99)	725–950	6	41.8	3.01	57.2	2.31	9.0
E_{eq} (MPa)	2.05 (1.84, 2.25)	700–1050	5	67.7	1.40	69.6	0.93	14.9
E_{dyn} (MPa)	9.44 (8.55, 10.32)	700–1050	5	68.9	5.90	67.1	3.83	14.3

The wavelength region and number of PLS components were optimized based on the root mean square error of prediction (RMSEP) and R^2 of test validation. The percentage error was determined as average error relative to the range of the reference variable. During the model development, R^2 and root mean square error of cross-validation (RMSECV) of the models were also determined. (CI = 95% confidence interval (lower limit, upper limit), C = number of PLS components, E_{in} = instantaneous modulus, E_{eq} = equilibrium modulus, E_{dyn} = dynamic modulus).

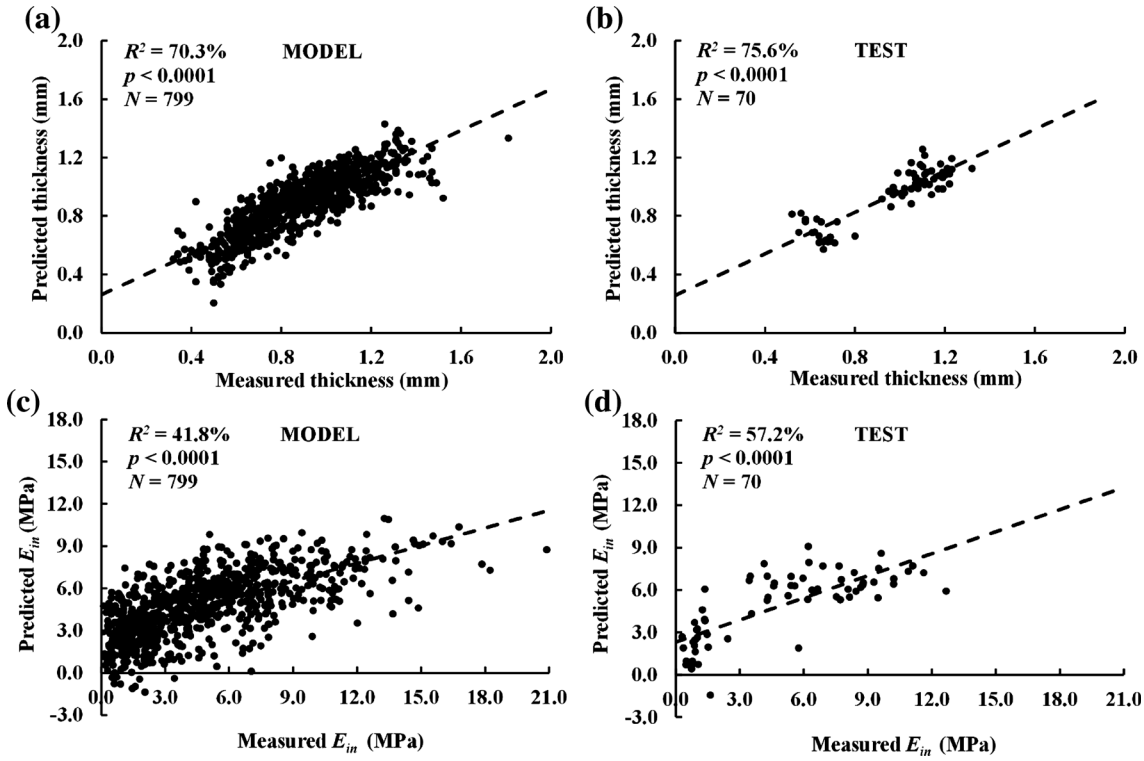

FIGURE 3. Partial least squares model and test correlations between preprocessed NIR spectral data and cartilage thickness (a, b) and instantaneous modulus (c, d) respectively.

Correlation between spectral data and cartilage properties were optimized in the NIR wavelength region (700–1150 nm). Prior to analysis, the visible (VIS) spectral region was inspected and excluded due to significant contribution of the subchondral bone to the absorption spectrum, especially in sites with thin cartilage layer. Furthermore, this region has been previously shown to correlate poorly with cartilage properties.[5] In this study, the absorption spectrum is assumed to include contributions from both tissues: cartilage and subchondral bone, as NIR penetration depth in equine cartilage is 3–5 mm.[18,35] Although, the spectral data includes latent information on both tissues, the effect of the overlying cartilage layer can be expected to be more profound and prominent owing to the high water content in cartilage.[8] However, the exact behaviour of light penetration into subchondral bone and reflection/scattering at the bone-cartilage interface are yet to be fully understood. Thus, further investigation, possibly through modeling of light interactions and depth-resolved spectroscopy are required. However, these are beyond the scope of the current study. Additionally, although extended NIR spectral range (1100–2500 nm) has been demonstrated to be effective for estimation of cartilage PG and collagen content in previous studies[6,33,37]; nevertheless it

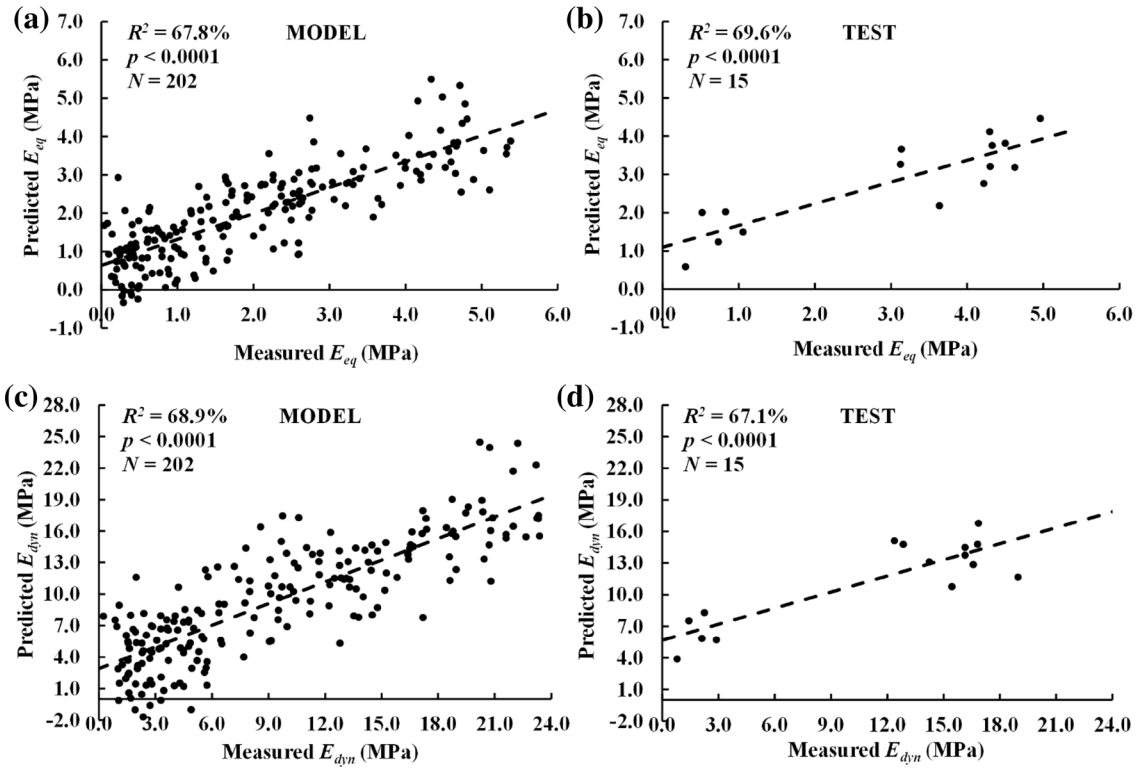

FIGURE 4. Partial least squares model and test correlations between preprocessed NIR spectral data and the equilibrium (a, b) and dynamic modulus (c, d) respectively.

is known that the masking effect of water absorption increases as wavelength increases,[36] with associated decrease in penetration depth into cartilage.

Variations in the spectral response are due to cartilage structure and composition where the main chemical bonds are associated with specific wavelength regions.[2,4,35,41] The OH bond of water is the most pronounced in the spectral response of articular cartilage[28,36] partly due to the abundant water content of the tissue. This can be observed in the prominent 3rd overtone absorption peak due to OH vibration around 970 nm (Fig. 2b). The correlation between spectral data and equilibrium modulus is likely due to swelling of damaged cartilage which results in increased free water content,[12,13] and hence the slightly higher peak. The baseline difference observed with varying thickness is due to path length effect, which is associated with the longer distance the light has to travel in thicker cartilage.[3] The third and fourth overtones of CH, SH, NH and OH, the common bonds of collagen and PG, are the other main characterizers of the absorbance. Therefore, the relationship between the optical properties of cartilage, its structure (components) and function (biomechanical response) is justifiable. A fourth overtone of OH stretch is detectable (Fig. 2b) around 750 nm. A slightly masked 3rd overtone peak, due to CH stretching vibration attributable to the solid matrix components of cartilage, can be observed at 910 nm. Nevertheless, adopting multivariate analysis allowed extraction of information from this peak *via* second derivative transformation.

Multilinear regression (MLR), principal component regression (PCR)[1] and partial least squares (PLS)[39] have been previously applied for spectral analysis. However, due to certain mathematical limitations, MLR breaks down when the number of variables exceeds certain threshold and cannot be successfully adapted for wide spectral analysis. PLS regression multivariate technique was employed for multivariate characterization and prediction instead of principal component analysis (PCA) or univariate analysis techniques. PLS enables a complete assessment of the spectra as opposed to univariate analyses where single wavelengths or area under peaks are considered.[9] Additionally, PCA is most suitable for dividing samples into distinct groups as an unsupervised classification method.[1,33] Although there is a multivariate prediction approach based on PCA (principal component regression—PCR); this method has been shown to be less effective than the PLS regression.[3] For a justifiable conclusion, the number of components and

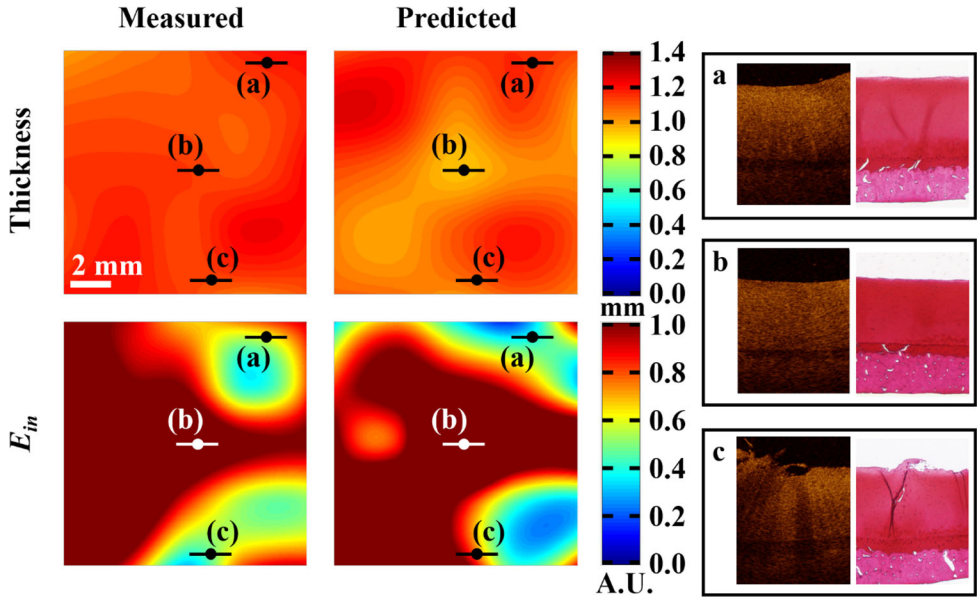

FIGURE 5. Spatial mapping of cartilage thickness and instantaneous modulus on one of the lesion AIs. The first and second rows present the cubic interpolated matrix of the thickness and instantaneous modulus, respectively. The measured and predicted instantaneous modulus are presented as normalized with the average instantaneous modulus to enhance the visualization of non-normal cartilage. Three locations (a–c) with corresponding OCT and histology images are indicated on the maps.

sample points both, R^2 and percentage error must be considered. In addition, decrease in model error is expected as the number of sample points increases.

Cartilage thickness is site-dependent and not a direct indicator of tissue health. However, severe degeneration often manifests as decrease in cartilage thickness, e.g., at lesion sites. Moderate cartilage lesion (Fig. 5c) is easily identified visually, but no significant variation is observable in the thickness maps, since significant changes in thickness are associated with advanced cartilage degeneration. The error in cartilage thickness prediction reported in this study (0.09 mm, 5.9%) is a fraction of the pixel size in clinical imaging modalities, such as MRI.[3,16] While the biomechanical properties of articular cartilage are indicative of the tissue condition, they are also patient- and site-specific[31]; thus, no absolute stiffness threshold can be defined for healthy and damaged cartilage (Fig. 5). However, a threshold for relative local decrease (compared to surrounding tissue) of cartilage stiffness could be determined for compromised cartilage. Both cartilage thickness and composition vary in disease; hence, as indicated in previous studies,[4,5,9] the adaptation of NIR spectroscopy for PG and collagen content is essential. Slight PG loss can be observed (Fig. 5a) in the histological image; although the corresponding OCT indicates healthy cartilage. This PG loss corresponds with compromised cartilage stiffness in the maps (Fig. 5a). Therefore, high-resolution imaging alone is insufficient to fully characterize cartilage condition. A site with severely damaged cartilage, as shown in the corresponding OCT and histological images (Fig. 5c), is indicated in the modulus map as a localised region with low stiffness. Slightly higher error can be observed in the instantaneous modulus map compared to the thickness map. Nevertheless, the predicted values are within the range of the measured values. However, the models still require further validation to improve prediction accuracy and errors for the different reference parameters.

This study demonstrates that the combination of NIR spectroscopy and PLS1 algorithm has the potential to facilitate rapid, objective, and non-destructive arthroscopic probing of cartilage mechanical properties with better reproducibility than hand-held arthroscopic indentation devices.[11,30] Although, the reproducibility of NIR has not been studied *in vivo,* the practicality of NIR probe is expected to be superior to hand-held indentation devices due to rapid data acquisition and easier measurement. Data acquisition and processing of a single measurement takes approximately 140 ms, therefore enabling adaptation of the method as a tool for *in vivo* mapping of cartilage properties. With further validation, this method could enable surgeons to map the damaged area around lesions during surgery and optimize the amount of degenerated tissue to be repaired during arthroscopic surgeries. Adaptation of similar mapping concept to human cartilage would require further experimentation and optimization with human samples—this is currently ongoing research in the group and we have recently published initial results showing the relation-

ship between optical response of human cartilage and its state of health.[5] However, the aim of the present study was to demonstrate a proof of concept of mapping the mechanical integrity of articular cartilage around lesion sites in equine joints.

The results in this study are well in line with previous studies.[3,5] Thickness, equilibrium and dynamic moduli correlate well with the spectral data. Although better correlations have been reported in earlier studies,[3,5] the extent of the research in previous studies were limited by the sample size and method of cross-validation compared to this study. The large amount of data ($N = 869$) in this study also resulted in wider variance between samples. The spectral range used in this study was limited by the equipment to the short NIR wavelength range, although the extended NIR range (1200–2500 nm) could provide more information on the parameters investigated in this study. Additionally, the exact contribution of subchondral bone to the overall osteochondral spectral information was not quantified in this study. However, the cartilage layer can be expected to be the main contributor to the spectral data owing to the high water content of the superficial layer.[4] The robust experimental setup with careful measurements ensured improved CV of spectral measurement compared to previous studies.[5,32] The moderate correlation ($R^2 = 41.8\%$) obtained with instantaneous modulus is possibly due to lower reproducibility of indentation compared to equilibrium and dynamic modulus measurements. CV of the measurement of instantaneous modulus with material testing equipment was 12.7%. In this study, the instantaneous modulus is highly influenced by the superficial cartilage as the indentation was initiated after the first contact of the indenter and cartilage surface. Therefore, it might not be optimal parameter for the determination of whole cartilage functional integrity. The equilibrium and dynamic modulus are less affected by the initial orientation due to better secured contact between indenter and cartilage with deeper indentation. In order to preserve sample integrity during measurements, the number of points measured with the 1st protocol was limited due to the amount of time required per measurements (half a joint: two 16 h measurement sessions).

In this study, conventional absorption spectroscopy technique was utilized. The resulting spectra include contribution from both cartilage and bone, but their specific contribution cannot be directly quantified or separated,[33] hence depth resolved spectroscopic techniques would be highly valuable. However, even with current advancements in technology, obtaining depth-wise information over a wide spectral range is not yet feasible arthroscopically. The implementation of the current hardware restricts the acquisition of a depth-resolved signal and is a limitation of the technique.

In conclusion, NIR spectral data correlates with non-calcified cartilage thickness and biomechanical properties, but the penetration of NIR light and its interaction in osteochondral tissues still require further investigations. The results obtained in this study suggest that NIR spectroscopy could enable estimation and mapping the biomechanical response of articular cartilage at and around lesions to be repaired during arthroscopic surgery.

ACKNOWLEDGMENTS

We acknowledge Dr Jouni Hiltunen, Dr Juha Toivonen and Prof Adekunle Oloyede for assistance with the optical instrumentation. This study was funded by the Academy of Finland (project 267551, University of Eastern Finland) and Kuopio University Hospital (VTR projects 5041750 and 5041744, PY210 Clinical Neurophysiology). Dr Afara would like to acknowledge the Finnish Cultural Foundation (00160079).

AUTHOR CONTRIBUTIONS

J.K. Sarin was involved in equine *ex vivo* study, data acquisition, analyses and was the main writer of the manuscript. M. Amissah contributed in the reference measurements. H. Brommer contributed in equine *ex vivo* study, equine arthroscopies. D. Argüelles contributed in equine *ex vivo* study, equine arthroscopies. J. Töyräs contributed in the study conception, equine *ex vivo* study, and interpretation of data. I.O. Afara contributed in the study conception, equine *ex vivo* study, data analyses and interpretation. All authors contributed in the preparation and approval of the final submitted manuscript.

CONFLICT OF INTEREST

The authors have no conflicts of interest in the execution of this study and preparation of the manuscript.

REFERENCES

[1]Afara, I. O., I. Prasadam, R. Crawford, Y. Xiao, and A. Oloyede. Non-destructive evaluation of articular cartilage defects using near-infrared (NIR) spectroscopy in osteoarthritic rat models and its direct relation to Mankin score. *Osteoarthritis Cartilage* 20:1367–1373, 2012.

[2]Afara, I. O., I. Prasadam, R. Crawford, Y. Xiao, and A. Oloyede. Near infrared (NIR) absorption spectra correlates with subchondral bone micro-CT parameters in osteoarthritic rat models. *Bone* 53:350–357, 2013.
[3]Afara, I. O., S. Singh, and A. Oloyede. Application of near infrared (NIR) spectroscopy for determining the thickness of articular cartilage. *Med. Eng. Phys.* 35:88–95, 2013.
[4]Afara, I. O., I. Prasadam, H. Moody, R. Crawford, Y. Xiao, and A. Oloyede. Near infrared spectroscopy for rapid determination of Mankin score components: a potential tool for quantitative characterization of articular cartilage at surgery. *Arthroscopy* 30:1146–1155, 2014.
[5]Afara, I. O., M. Hauta-Kasari, J. S. Jurvelin, A. Oloyede, and J. Töyräs. Optical absorption spectra of human articular cartilage correlate with biomechanical properties, histological score and biochemical composition. *Physiol. Meas.* 36:1913–1928, 2015.
[6]Afara, I. O., H. Moody, S. Singh, I. Prasadam, and A. Oloyede. Spatial mapping of proteoglycan content in articular cartilage using near-infrared (NIR) spectroscopy. *Biomed. Opt. Express* 6:144–154, 2015.
[7]Ala-Myllymäki, J., J. T. J. Honkanen, J. Töyräs, and I. O. Afara. Optical spectroscopic determination of human meniscus composition. *J. Orthop. Res.* 18:109–115, 2015.
[8]Amin, S., M. P. LaValley, A. Guermazi, M. Grigoryan, D. J. Hunter, M. Clancy, J. Niu, D. R. Gale, and D. T. Felson. The relationship between cartilage loss on magnetic resonance imaging and radiographic progression in men and women with knee osteoarthritis. *Arthritis Rheum.* 52:3152–3159, 2005.
[9]Baykal, D., O. Irrechukwu, P.-C. Lin, K. Fritton, R. G. Spencer, and N. Pleshko. Nondestructive assessment of engineered cartilage constructs using near-infrared spectroscopy. *Appl. Spectrosc.* 64:1160–1166, 2010.
[10]Brittberg, M., and C. S. Winalski. Evaluation of cartilage injuries and repair. *J. Bone Joint Surg. Am.* 85-A(Suppl 2):58–69, 2003.
[11]Brommer, H., M. S. Laasanen, P. A. J. Brama, P. R. van Weeren, H. J. Helminen, and J. S. Jurvelin. In situ and ex vivo evaluation of an arthroscopic indentation instrument to estimate the health status of articular cartilage in the equine metacarpophalangeal joint. *Vet. Surg.* 35:259–266, 2006.
[12]Buckwalter, J. A., and T. D. Brown. Joint injury, repair, and remodeling: roles in post-traumatic osteoarthritis. *Clin. Orthop. Relat. Res.* 423:7–16, 2004.
[13]Buckwalter, J. A., and H. J. Mankin. Articular cartilage: degeneration and osteoarthritis, repair, regeneration, and transplantation. *Instr. Course Lect.* 47:487–504, 1998.
[14]Burns, D. A., and E. W. Ciurczak. Handbook of Near-Infrared Analysis (3rd ed.). Boca Raton: CRC Press, 2009.
[15]Chu, C. R., D. Lin, J. L. Geisler, C. T. Chu, F. H. Fu, and Y. Pan. Arthroscopic microscopy of articular cartilage using optical coherence tomography. *Am. J. Sports Med.* 32:699–709, 2004.
[16]Cohen, Z. A., D. M. McCarthy, S. D. Kwak, P. Legrand, F. Fogarasi, E. J. Ciaccio, and G. A. Ateshian. Knee cartilage topography, thickness, and contact areas from MRI: in vitro calibration and in vivo measurements. *Osteoarthristis Cartilage* 7:95–109, 1999.
[17]De Souza, R. A., M. Xavier, N. M. Mangueira, A. P. Santos, A. L. B. Pinheiro, A. B. Villaverde, and L. Silveira. Raman spectroscopy detection of molecular changes associated with two experimental models of osteoarthritis in rats. *Lasers Med. Sci.* 29:797–804, 2014.
[18]Ebert, D. W. Articular Cartilage Optical Properties in the Spectral Range 300–850 nm. *J. Biomed. Opt.* 3:326, 1998.
[19]Glüer, C. C., G. Blake, Y. Lu, B. A. Blunt, M. Jergas, and H. K. Genant. Accurate assessment of precision errors: how to measure the reproducibility of bone densitometry techniques. *Osteoporos. Int.* 5:262–270, 1995.
[20]Hanifi, A., X. Bi, X. Yang, B. Kavukcuoglu, P. C. Lin, E. DiCarlo, R. G. Spencer, M. P. G. Bostrom, and N. Pleshko. Infrared fiber optic probe evaluation of degenerative cartilage correlates to histological grading. *Am. J. Sports Med.* 40:2853–2861, 2012.
[21]Haq, I., E. Murphy, and J. Dacre. Osteoarthritis. *Postgrad. Med. J.* 79:377–383, 2003.
[22]Hattori, K., K. Ikeuchi, Y. Morita, and Y. Takakura. Quantitative ultrasonic assessment for detecting microscopic cartilage damage in osteoarthritis. *Arthritis Res. Ther.* 7:R38–R46, 2005.
[23]Hayes, W. C., L. M. Keer, G. Herrmann, and L. F. Mockros. A mathematical analysis for indentation tests of articular cartilage. *J. Biomech.* 5:541–551, 1972.
[24]Hunziker, E. B. Articular cartilage repair: basic science and clinical progress. A review of the current status and prospects. *Osteoarthritis Cartilage* 10:432–463, 2002.
[25]Huttu, M. R. J., J. Puhakka, J. T. A. Mäkelä, Y. Takakubo, V. Tiitu, S. Saarakkala, Y. T. Konttinen, I. Kiviranta, and R. K. Korhonen. Cell-tissue interactions in osteoarthritic human hip joint articular cartilage. *Connect. Tissue Res.* 55:282–291, 2014.
[26]Korhonen, R., M. Laasanen, J. Töyräs, J. Rieppo, J. Hirvonen, H. Helminen, and J. Jurvelin. Comparison of the equilibrium response of articular cartilage in unconfined compression, confined compression and indentation. *J. Biomech.* 35:903–909, 2002.
[27]Korhonen, R. K., M. S. Laasanen, J. Töyräs, R. Lappalainen, H. J. Helminen, and J. S. Jurvelin. Fibril reinforced poroelastic model predicts specifically mechanical behavior of normal, proteoglycan depleted and collagen degraded articular cartilage. *J. Biomech.* 36:1373–1379, 2003.
[28]Lai, W. M., J. S. Hou, and V. C. Mow. A triphasic theory for the swelling and deformation behaviors of articular cartilage. *J. Biomech. Eng.* 113:245–258, 1991.
[29]Lee, H., W. G. Kirkland, R. N. Whitmore, K. M. Theis, H. E. Young, A. J. Richardson, R. L. Jackson, and R. R. Hanson. Comparison of equine articular cartilage thickness in various joints. *Connect. Tissue Res.* 55:339–347, 2014.
[30]Lyyra, T., J. Jurvelin, P. Pitkänen, U. Väätäinen, and I. Kiviranta. Indentation instrument for the measurement of cartilage stiffness under arthroscopic control. *Med. Eng. Phys.* 17:395–399, 1995.
[31]Mäkelä, J. T. A., Z. S. Rezaeian, S. Mikkonen, R. Madden, S.-K. Han, J. S. Jurvelin, W. Herzog, and R. K. Korhonen. Site-dependent changes in structure and function of lapine articular cartilage 4 weeks after anterior cruciate ligament transection. *Osteoarthritis Cartilage* 22:869–878, 2014.
[32]McGoverin, C. M., A. Hanifi, U. P. Palukuru, F. Yousefi, P. B Glenn, M. Shockley, R. G. Spencer, and N. Pleshko. Non-destructive assessment of engineered cartilage composition by near infrared spectroscopy. *Ann. Biomed. Eng.* 44(3):680–692, 2016.
[33]McGoverin, C. M., K. Lewis, X. Yang, M. P. G. Bostrom, and N. Pleshko. The Contribution of Bone and Cartilage to the Near-Infrared Spectrum of Osteochondral Tissue. *Appl. Spectrosc.* 68:1168–1175, 2014.

[34]Mow, V. C., A. Ratcliffe, and A. R. Poole. Cartilage and diarthrodial joints as paradigms for hierarchical materials and structures. *Biomaterials* 13:67–97, 1992.
[35]Padalkar, M. V., and N. Pleshko. Wavelength-dependent penetration depth of near infrared radiation into cartilage. *Analyst* 140:2093–2100, 2015.
[36]Padalkar, M. V., R. G. Spencer, and N. Pleshko. Near infrared spectroscopic evaluation of water in hyaline cartilage. *Ann. Biomed. Eng*. 41:2426–2436, 2013.
[37]Palukuru, U. P., C. M. McGoverin, and N. Pleshko. Assessment of hyaline cartilage matrix composition using near infrared spectroscopy. *Matrix Biol*. 38:3–11, 2014.
[38]Reinikainen, S.-P., and A. Höskuldsson. Multivariate statistical analysis of a multi-step industrial processes. *Anal. Chim. Acta* 595:248–256, 2007.
[39]Rieppo, L., S. Saarakkala, T. Närhi, H. J. Helminen, J. S. Jurvelin, and J. Rieppo. Application of second derivative spectroscopy for increasing molecular specificity of fourier transform infrared spectroscopic imaging of articular cartilage. *Osteoarthristis Cartilage* 20:451–459, 2012.
[40]Saarakkala, S., M. S. Laasanen, J. S. Jurvelin, and J. Töyräs. Quantitative ultrasound imaging detects degenerative changes in articular cartilage surface and subchondral bone. *Phys. Med. Biol*. 51:5333–5346, 2006.
[41]Spahn, G., H. Plettenberg, E. Kahl, H. M. Klinger, T. Mückley, and G. O. Hofmann. Near-infrared (NIR) spectroscopy. A new method for arthroscopic evaluation of low grade degenerated cartilage lesions. Results of a pilot study. *BMC Musculoskelet. Disord*. 8:47, 2007.
[42]Spahn, G., H. M. Klinger, and G. O. Hofmann. How valid is the arthroscopic diagnosis of cartilage lesions? Results of an opinion survey among highly experienced arthroscopic surgeons. *Arch. Orthop. Trauma Surg*. 129:1117–1121, 2009.
[43]Spahn, G., H. M. Klinger, M. Baums, U. Pinkepank, and G. O. Hofmann. Reliability in arthroscopic grading of cartilage lesions: results of a prospective blinded study for evaluation of inter-observer reliability. *Arch. Orthop. Trauma Surg*. 131:377–381, 2011.
[44]Spahn, G., G. Felmet, and G. O. Hofmann. Traumatic and degenerative cartilage lesions: arthroscopic differentiation using near-infrared spectroscopy (NIRS). *Arch. Orthop. Trauma Surg*. 133:997–1002, 2013.
[45]Takahashi, Y., N. Sugano, M. Takao, T. Sakai, T. Nishii, and G. Pezzotti. Raman spectroscopy investigation of load-assisted microstructural alterations in human knee cartilage: preliminary study into diagnostic potential for osteoarthritis. *J. Mech. Behav. Biomed. Mater*. 31:77–85, 2014.
[46]Te Moller, N. C. R., H. Brommer, J. Liukkonen, T. Virén, M. Timonen, P. H. Puhakka, J. S. Jurvelin, P. R. van Weeren, and J. Töyräs. Arthroscopic optical coherence tomography provides detailed information on articular cartilage lesions in horses. *Vet. J*. 197:589–595, 2013.
[47]Töyräs, J., J. Rieppo, M. T. Nieminen, H. J. Helminen, and J. S. Jurvelin. Characterization of enzymatically induced degradation of articular cartilage using high frequency ultrasound. *Phys. Med. Biol*. 44:2723–2733, 1999.
[48]Von Engelhardt, L. V., M. Lahner, A. Klussmann, B. Bouillon, A. Dàvid, P. Haage, and T. K. Lichtinger. Arthroscopy vs. MRI for a detailed assessment of cartilage disease in osteoarthritis: diagnostic value of MRI in clinical practice. *BMC Musculoskelet. Disord*. 11:75, 2010.
[49]Wold, S., M. Sjöström, and L. Eriksson. PLS-regression: a basic tool of chemometrics. *Chemom. Intell. Lab. Syst*. 58:109–130, 2001.
[50]Yin, J., and Y. Xia. Proteoglycan concentrations in healthy and diseased articular cartilage by Fourier transform infrared imaging and principal component regression. *Spectrochim. Acta A Mol. Biomol. Spectrosc*. 133:825–830, 2014.